

## Multiple-bandwidth photoacoustic tomography

Geng Ku<sup>1</sup>, Xueding Wang<sup>1</sup>, George Stoica<sup>2</sup> and Lihong V Wang<sup>1</sup>

<sup>1</sup> Optical Imaging Laboratory, Department of Biomedical Engineering, Texas A&M University, 3120 TAMU, College Station, TX 77843-3120, USA

<sup>2</sup> Department of Pathobiology, Texas A&M University, College Station, TX 77843-5547, USA

E-mail: LWang@tamu.edu

Received 30 September 2003

Published 18 March 2004

Online at [stacks.iop.org/PMB/49/1329](http://stacks.iop.org/PMB/49/1329) (DOI: 10.1088/0031-9155/49/7/018)

### Abstract

Photoacoustic tomography, also referred to as optoacoustic tomography, employs short laser pulses to generate ultrasonic waves in biological tissues. The reconstructed images can be characterized by the convolution of the structure of samples, the laser pulse and the impulse response of the ultrasonic transducer used for detection. Although the laser-induced ultrasonic waves cover a wide spectral range, a single transducer can receive only part of the spectrum because of its limited bandwidth. To systematically analyse this problem, we constructed a photoacoustic tomographic system that uses multiple ultrasonic transducers simultaneously, each at a different central frequency. The photoacoustic images associated with the different transducers were compared and analysed. The system was tested by imaging both mouse brains and phantom samples. The vascular vessels in the brain were revealed by all of the transducers, but the image resolutions differed. The higher frequency detectors provided better image resolution while the lower frequency detectors delineated the major structural traits with a higher signal–noise ratio.

### Introduction

Photoacoustic tomography is a non-ionizing imaging modality for visualizing biological tissues with optical contrast and ultrasonic resolution. The induced acoustic signals from biological tissues exhibit heterogeneity of optical absorption in the samples and reveal the structure of tissues. For some specified wavelength of light, the absorption coefficient of blood can be 10 times higher than that of its surrounding tissues (Hoelen *et al* 1998). Because fast developing tumours consume more blood, most malignant tumours have higher optical absorption. For example, the absorption contrast between breast tumours and normal breast tissues can be as high as 300% at the 1064 nm wavelength (Oraevsky *et al* 1999). Another example is represented by the tumours of the nervous system, which in general are well vascularized, especially the most malignant ones such as glioblastoma multiforme (GBM).

GBM is characterized by an increased vascular proliferation, cellular heterogeneity and necrosis. These characteristics reflect rich and distorted vasculature within the tumour. Intra-tumoural arteriovenous shunting and early filling of draining cerebral veins are commonly seen due to tumour-related neovascularization (Nelson and Cha 2003). The laser-induced thermal expansion of an absorptive structure in tissues creates acoustic waves by the thermoelastic mechanism. The induced acoustic waves spread out through the medium and can be detected by ultrasonic detectors. Photoacoustic imaging is based on ultrasonic propagation and detection, which means that it has the same good spatial resolution as pure ultrasound imaging.

The geometry of the region over which the ultrasonic transducer is scanned determines the imaging mode and the reconstruction algorithms. For the detection of layered structures of tissues or tumours under human epidermis, the ultrasonic transducer has to be placed on the skin along the laser beam to accomplish detection *in vivo*. Karabutov *et al* (1999, 2000) presented photoacoustic imaging with axial resolution up to 15  $\mu\text{m}$ . The imaging of small deeply embedded tumours, such as breast tumours, was also studied by Esenaliev *et al* (1999) and Oraevsky *et al* (1999) (Esenaliev *et al* 1997). Hoelen *et al* employed a transducer array on a plane to detect induced signals from vascular systems (Hoelen and de Mul 2000). The image was reconstructed using a delay-and-sum algorithm, where the depth resolution was better than 20  $\mu\text{m}$ , and the lateral resolution was better than 200  $\mu\text{m}$ . The detector can also scan over a circle (Kruger *et al* 1995). Some reconstruction algorithms have been developed to use the signals from the scan to form an image. Examples of current reconstruction algorithms include the weighted delay-and-sum method (Esenaliev *et al* 1997), the optimal statistical approach (Zhulina 2000) and the Radon transform in the far-field approximation (Kruger *et al* 1999). Only recently have exact reconstructions been studied theoretically and reconstruction algorithms for various regular geometries derived (Kostli *et al* 2001, Xu and Wang 2002, Xu *et al* 2002a, Xu *et al* 2002b).

The generation, propagation and detection of induced acoustic signals can be described by thermal expansion, wave equations and bandwidth filtering, respectively (Ku and Wang 2000). By directing the laser pulse on a test sample, the absorbed optical energy in tissue is transformed into thermal energy, which is then, due to thermoelastic expansion, converted into mechanical stress. If the energy deposition occurs rapidly in a time period that is much less than the thermal relaxation time and the stress relaxation time, the local pressure rise after heating can be derived as  $\Delta p = \frac{\beta c^2}{C_p} E_a$ , where  $\Delta p$  is the pressure rise,  $\beta$  is the isobaric volume expansion coefficient,  $c$  is the speed of sound,  $C_p$  is the specific heat, and  $E_a$  is the absorbed optical energy density.

The behaviour of photoacoustic waves has been studied by Diebold and Gusev *et al* based on the following non-homogenous wave equation (Diebold *et al* 1992, Gusev and Karabutov 1993):

$$\nabla^2 p(\mathbf{r}, t) - \frac{1}{c^2} \frac{\partial^2 p(\mathbf{r}, t)}{\partial t^2} = -\frac{\beta}{C_p} \frac{\partial H(\mathbf{r}, t)}{\partial t} \quad (1)$$

where  $p(\mathbf{r}, t)$  is the acoustic pressure at time  $t$  and position  $\mathbf{r}$  and  $H(\mathbf{r}, t)$  is the heat function of the optical energy deposited in the tissues per unit volume per unit time, which can be expressed as

$$H(\mathbf{r}, t) = A(\mathbf{r})I(t) \quad (2)$$

where  $A(\mathbf{r})$  describes the optical energy deposition within the tissues at position  $\mathbf{r}$  (structure of tissues); and  $I(t)$  describes the shape of the irradiation pulse, which can be further expressed as  $I(t) = \delta(t)$  for impulse heating.

The purpose of photoacoustic tomography is to reconstruct the distribution of the optical absorption  $A(\mathbf{r})$  in the tissues from a set of measured acoustic signals  $p(\mathbf{r}, t)$ . For a cylindrical

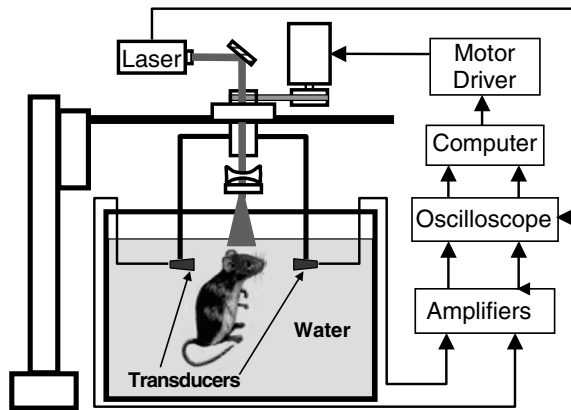


**Figure 1.** Experimental set-up of photoacoustic tomography employing multiple ultrasonic transducers, each at a different frequency.

scanning configuration, the exact inverse solution can be derived. In most practical image reconstruction, the algorithm can be simplified to shorten the reconstruction time. If the detection radius  $r_0$  is much longer than the wavelength that corresponds to the central frequency of the detection device (far-field detection), we can assume  $|k|r_0 \gg 1$  and simplify the exact inverse solution to the form of (Xu *et al* 2003)

$$A(\mathbf{r}) = -\frac{\beta}{2\pi c^4 C_p} \int_{S_0} \int dS_0 (\cos \Theta) \frac{1}{t} \frac{\partial p(\mathbf{r}_0, t)}{\partial t} \Big|_{t=|r_0-\mathbf{r}|/c} \quad (3)$$

where  $S_0$  is the surface over which the detectors are scanned,  $\Theta$  is the angle between the normal line of the detector and the vector from the detector to the reconstruction point.

Induced acoustic waves range widely in the frequency spectrum. However, a single ultrasonic transducer can only respond to part of the spectrum because of its limited bandwidth (Ku and Wang 2001). In general, a transducer with a higher central frequency detects acoustic signals with a wider bandwidth, but the signal is weaker. Sometimes choosing the ultrasonic detector is a dilemma since a trade-off between imaging resolution (bandwidth) and sensitivity may be necessary. In this paper, we demonstrate a photoacoustic imaging experiment that simultaneously uses three transducers with the 3.5 MHz, 10 MHz and 20 MHz central frequencies, respectively. Images associated with the three transducers will be compared and analysed. Further discussions on image resolution and signal–noise ratio (SNR) will be presented as well.

## 1. Experimental set-up

The experimental set-up for the photoacoustic tomographic system employing multiple ultrasonic transducers is shown in figure 1. A Q-switched pulsed Nd:YAG laser (Brilliant B, BigSky), operating at the second harmonic wave with a wavelength of 532 nm, is used as the pumping source. The laser pulse width is 6.5 ns and the pulse repetition rate is 10 Hz. The laser beam is expanded by a concave lens and homogenized by a ground glass and then is delivered to the test sample. The pulse energy density is controlled below  $\sim 20 \text{ mJ cm}^{-2}$ , which is the maximum permissible exposure (MPE) for skin to a laser beam at a wavelength of 532 nm (ANSI 2000).

Three ultrasonic transducers (V383/3.5 MHz, XMS-310/10 MHz, and V316-N/20 MHz, Panametrics) are used as the detectors to receive the induced acoustic signals. The diameters of the active areas are 10 mm for the 3.5 MHz transducer, 2 mm for the 10 MHz transducer and 3 mm for the 20 MHz transducer, respectively. These commercial transducers have nominal bandwidths of 50% to 80% of their central frequencies.

A two-dimensional translation of the detectors is designed; one involves circular scanning in the horizontal plane, and the other involves linear scanning along the vertical direction. A rotational apparatus supported by two bearings is driven by a step motor to implement the circular scanning. The entire horizontal scanning section is made as one piece and then connected to an uprightly placed translation stage. Hence, the section of the circular scan can be impelled vertically. The transducers are attached to the rotational apparatus to complete circular scanning around the test sample. By combining the two movements, the transducers can scan in a cylindrical contour around the test sample (Wang *et al* 2003). However, we will report here only results based on one-dimensional circular scans. Typical scanning parameters in our experiment are 240 steps for a full view of  $2\pi$  circular scanning ( $1.5^\circ/\text{step}$ ) and 10 steps in 12.7 mm range (1.27 mm/step) for vertical scanning.

The transducers convert the acoustic energy into electrical signals that are amplified by amplifiers (ZFL-500LN, Mini-Circuits). An oscilloscope with four channels (TDS-540A, Tektronix) is employed to monitor and record the acoustic signals. A LabView program controls the scanning of the transducers and the data acquisition according to the following sequence: first, start the step motor to move the transducers to the arranged position; secondly, fire the laser and trigger the data acquisition; third, average the time-dependant signals on the oscilloscope to improve the SNR; finally, save the time-dependent data at this scanning stop. After that, the transducers are moved to the next scanning stop and the above procedure is repeated.

For coupling the induced acoustic signals, the transducers and the test sample are immersed in water in a container. The laser light is directed onto the test sample through a hole on the rotational axis. The head of an adult BALB/c mouse (Charles River Breeding Laboratories,  $\sim 27$  g) was imaged using the above-mentioned three transducers simultaneously. The hair on the mouse head was removed gently using hair remover lotion to improve light penetration.

## 2. Results and discussion

The resolution of photoacoustic imaging is primarily limited by the bandwidth of the detector and the laser pulse duration. Theoretically, the structure of tissues with optical absorption contrast can in most cases be either exactly reconstructed or approximately reconstructed by equation (3). The pressure engaged in the equation is supposed to cover the whole spectrum; and, indeed, the induced photoacoustic signal is rather wide although only part of its spectra can be detected by the single transducer. Using the signals from a limited bandwidth detector causes the reconstructed image to blur. In addition, the reconstructed structure of tissues can also be blurred by the duration of laser pulse, which is assumed to be a delta stimulation in the derivation of the reconstruction equation (3). Accordingly, the reconstructed image is affected by the convolution of the structure of tissues in optical absorption, the profile of the pumping pulse, and the impulse response of the detector,

$$I(r) = S(r) * L(t \cdot c) * D(t \cdot c) \quad (4)$$

where, convolution is denoted by  $*$ ;  $I(r)$  characterizes the reconstructed image;  $S(r)$  represents the optical structure of tissues;  $L(t \cdot c)$  and  $D(t \cdot c)$  are the laser pulse and transducer impulse

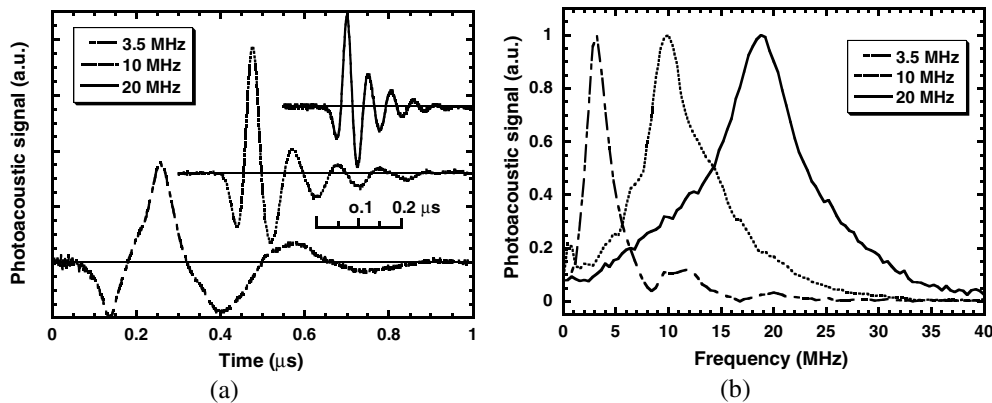


**Figure 2.** Impulse responses of the ultrasonic transducers stimulated by a laser pulse in (a) the time domain and (b) the frequency domain.

responses converted to the spatial domain. The bell-shaped laser pulse is 6.5 ns wide in our experiments and blurs the structure of tissues by  $\sim 10 \mu\text{m}$ .

The effect of an ultrasonic transducer on the detected photoacoustic signals can be investigated by the impulse response. Figure 2(a) shows the measured impulse responses accomplished by illuminating the laser pulse onto the transducers and stimulating ultrasonic waves on the surface of the transducers. The effects of the duration of the laser pulse and the limited bandwidth of the ultrasonic transducer are combined in this measurement, which provides a system response. The corresponding spectra are shown in figure 2(b). Each profile of the impulse responses presents an initial negative lobe, transits to a positive main lobe, and then oscillates to zero.

To examine the image resolution, we made a phantom sample that is a cross of two mouse hairs in a block of transparent gel (5% gelatin). The photoacoustic images obtained by the three transducers are shown in figures 3(a)–(c). Three one-dimensional images of one of the hair fibres, whose diameter is  $\sim 60 \mu\text{m}$ , are plotted in figure 3(d), where the  $x$  axis is shifted to align the peaks. The profile corresponding to the higher frequency transducer is narrower, which indicates higher image resolution. Comparing the reconstructed images in figures 3(a)–(c) and the one-dimensional images in figure 3(d), most viewers take the positive main lobe to be the visual object. We here define the resolution of an image as the width of the main lobe crossing zero minus the width of the imaged hair. Here, we checked the image on a cross section of a hair fibre. The zero-crossing widths of the positive main lobes of the reconstructed images are  $270 \mu\text{m}$ ,  $120 \mu\text{m}$  and  $90 \mu\text{m}$  for the three transducers: 3.5 MHz, 10 MHz, and 20 MHz, respectively. As discussed in the preceding text, the image of an object is a convolution between the real size of the object and the point spread function of the imaging system. For simplicity, if the diameter of the hair ( $60 \mu\text{m}$ ) is subtracted from the widths of the main lobes, the corresponding image resolutions appeared to be approximately  $210 \mu\text{m}$ ,  $60 \mu\text{m}$  and  $30 \mu\text{m}$  for the above three transducers, respectively. Therefore, an ultrasonic transducer with a higher central frequency and a broader bandwidth generally provides better spatial resolution, which is consistent with the theoretical analysis of the frequency dependence of spatial resolution (Xu and Wang 2003).

The aperture of the transducer causes its impulse response to be a function of spatial variables. If the aperture is less than the detected ultrasonic wavelength, the detector approaches a point detector and thus becomes omnidirectional. However, the detector's sensitivity can be augmented by increasing its active areas. The active sizes of the transducers

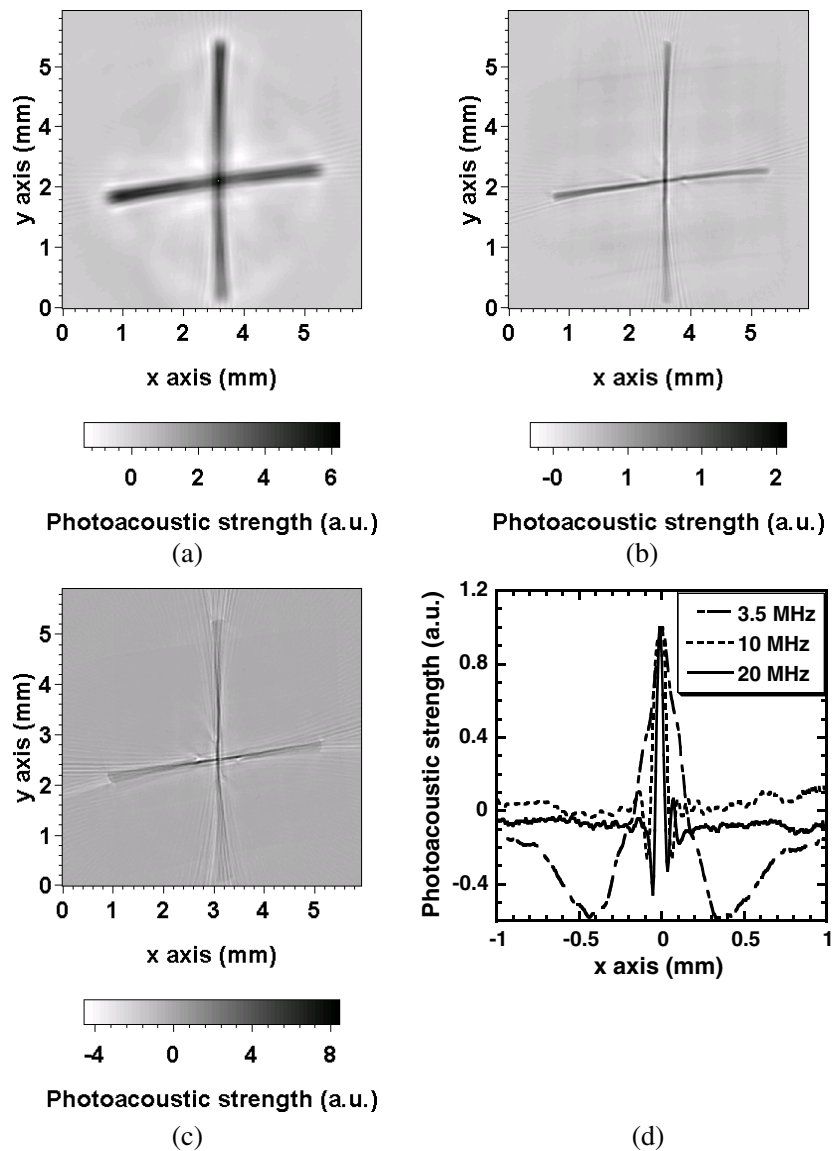


**Figure 3.** Photoacoustic images of a cross made by two mouse hairs acquired with (a) the 3.5 MHz transducer, (b) the 10 MHz transducer and (c) the 20 MHz transducer. The dark area in the image represents stronger photoacoustic signal. (d) One-dimensional photoacoustic images of a cross section of the hair fibre of  $60\ \mu\text{m}$  in diameter by the three transducers.

in our experiment are not negligible, consequently, cannot be treated as point detectors; therefore, the impulse responses depend on the position of the photoacoustic source. A heuristic understanding is that the distance between an ultrasonic source in space and a point on the ultrasonic detector with a certain aperture varies with the location of this point on the surface of the detector. This variation causes a variation in the phase of the detected photoacoustic signals which broadens the impulse response. When the transducer scans over the circle, the impulse response remains the same only for the centre of the circle. When the ultrasonic source is off the centre, the impulse response varies as the transducer is scanned.

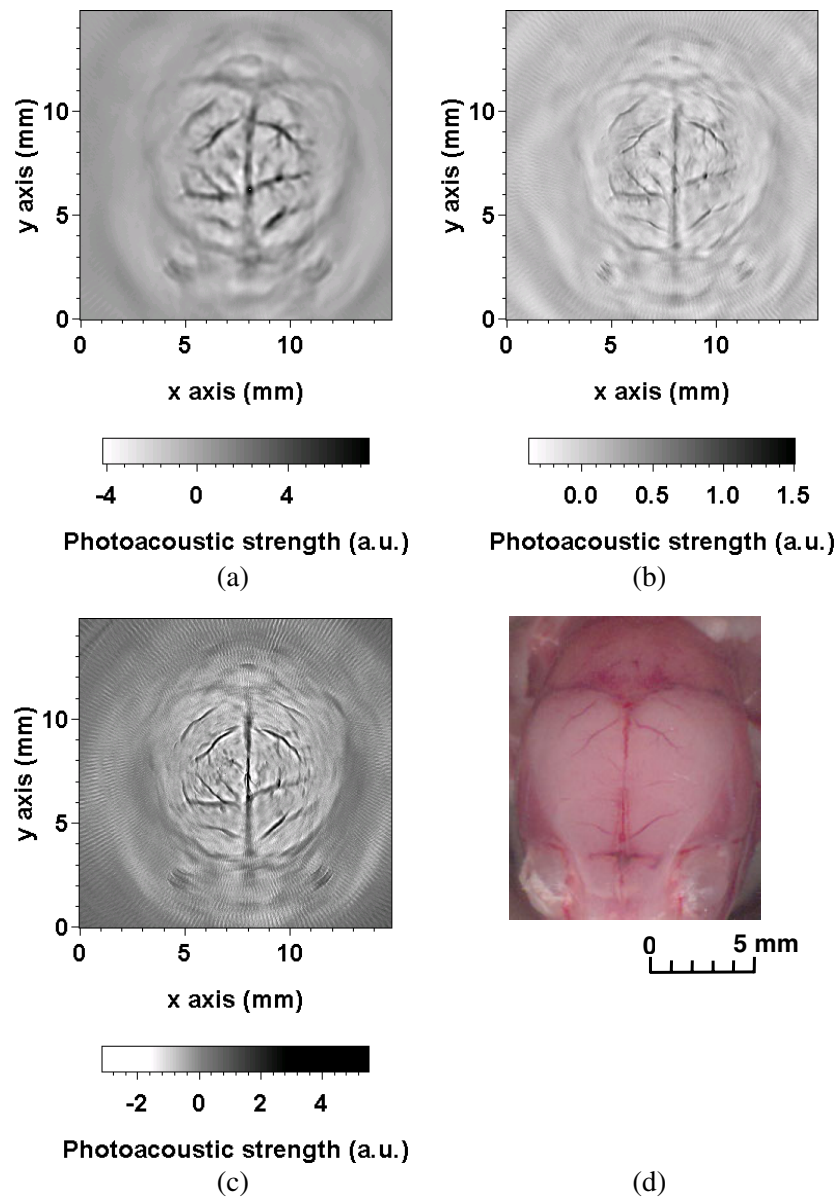


**Figure 4.** Photoacoustic images of a mouse brain acquired with (a) the 3.5 MHz transducer, (b) the 10 MHz transducer and (c) the 20 MHz transducer. (d) Top-view photograph of the mouse brain where the scalp was stripped after the photoacoustic imaging. (e)–(h) Close-ups of (a)–(d). The dark area in the image represents stronger photoacoustic signal.

(This figure is in colour only in the electronic version)

The farther off the ultrasonic source is from the centre, the wider the variation of the impulse response. As a result, the image resolution deteriorates with an increase in the distance from the centre of rotation. Xu and Wang deduced and predicted this aperture effect mathematically (Xu and Wang 2003). The aperture effect is obvious in figures 3(a)–(c), where the hair fibres are clear in the central area of the image, then become broader towards the far ends.

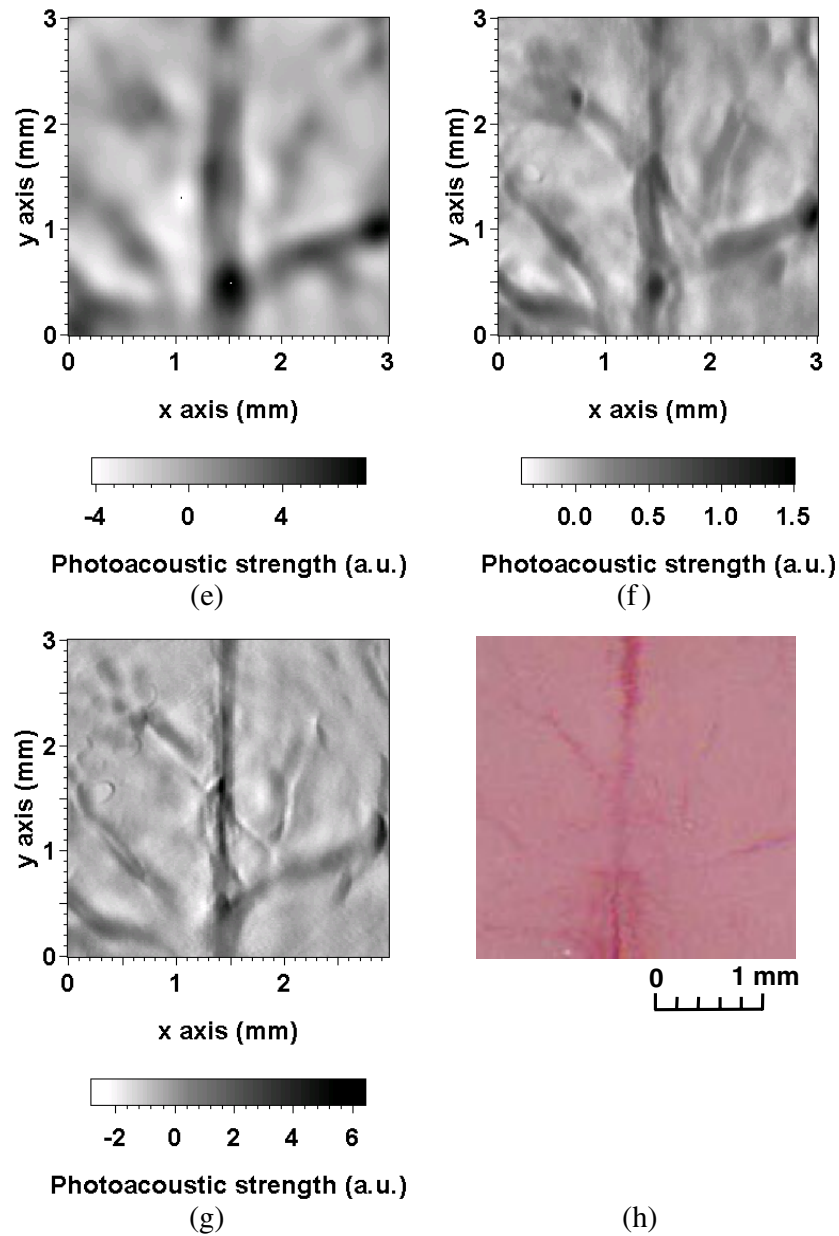


Figure 4. (Continued.)

The photoacoustic images of a mouse brain obtained by the three ultrasonic transducers are shown in figures 4(a)–(c), respectively. The images are compared with the open-scalp photograph of the mouse brain shown in figure 4(d) that was taken after the photoacoustic imaging. The vessels in the upper cerebral cortex provide the primary photoacoustic source because the laser light is directed to the top of the mouse head and the blood in the vessels has a high optical absorption coefficient at this wavelength. The skull and scalp as well as the other brain tissues around the upper cerebral vessels have much smaller optical absorption

coefficients. Light attenuation further reduces the absorbed optical energy density below the cortex. On the detection side, the photoacoustic sources in the imaging plane are preferentially detected. The diameters of the ultrasonic transducers are greater than their detected ultrasonic wavelengths and cause receiving directionalities; as a result, the effective zone of detection in the imaging area is  $\sim 4$  mm along the vertical axis. The combined effect of the optical and ultrasonic selectivities produced the clear photoacoustic images of the upper cerebral blood vessels.

By comparing the photoacoustic images with the anatomical photograph, some image properties that correlate with the detection spectra become evident. First, the main vessels on the cortex are disclosed by all three photoacoustic images. The photoacoustic signal covers a broad spectrum and the signal with a limited bandwidth does succeed in recording some of the characteristics of the object regardless of the bandwidth. Secondly, the detected signal from the lower frequency transducer is stronger, so the SNR of the image is better; but its resolution is poorer. In the image obtained by the 3.5 MHz transducer, every trait shows a feature in the mouse brain although the detailed structure is blurred. Thirdly, higher frequency detectors provide better image resolution as expected. For an identical vessel, the image obtained by the 3.5 MHz transducer is thicker than those obtained by the other two higher frequency transducers. The tiny vessels in the central area and some vascular ramifications spreading from the main vessels are perceptible in the image obtained by the 20 MHz transducer but can hardly be seen in the image obtained by the 10 MHz transducer and are totally blurred in the image obtained by the 3.5 MHz transducer. The close-up images reveal the resolution difference more clearly in figures 4(e)–(h).

The reconstruction improves the SNR of images. The excited ultrasonic signals will appear in the time-dependant signals recorded at all the scanning stops. In the reconstruction algorithm, the received signal amplitude is compensated for by a distance-related factor for each scanning stop. These compensated signals are properly time delayed and summed. For the scanning centre and its adjacent area, the summed signal increases approximately by  $N_s$  in its amplitude, where  $N_s$  is the number of scanning stops. The summed noise increases by only  $\sqrt{N_s}$  because of the random characteristic of the noise. So the SNR of the reconstructed image increases approximately  $\sqrt{N_s}$  compared with that of a single received ultrasonic signal. If the ultrasonic signal is averaged  $N_r$  times, the SNR of the reconstructed image is improved by  $\sqrt{N_s N_r}$  in total. In the above experiments,  $N_s$  was 240 and  $N_r$  was 10 and 50 for the hair imaging and the mouse imaging, respectively. As a consequence, the SNR was improved approximately 49 and 110 times, correspondingly.

### 3. Conclusion

Employing ultrasonic transducers of various bandwidths, two-dimensional photoacoustic tomography successfully reveals the vascular structures of the cortex in the mouse brain with various traits. We demonstrated that a higher frequency ultrasonic transducer gives a higher resolution image while a lower frequency transducer provides images with a higher signal–noise ratio. The image resolutions appeared to be approximately  $210 \mu\text{m}$ ,  $60 \mu\text{m}$  and  $30 \mu\text{m}$  for the transducers of 3.5 MHz, 10 MHz, and 20 MHz, respectively. In clinical imaging applications, tumours and other tissues are likely to have complicated shapes and optical absorptions. Consequently, the acoustic signals will have wide spectra. It will be difficult to set the detection bandwidth optimally in advance. The use of multiple transducers, each differing in the central frequency, is a superior method for capturing the images which cover a wide spectrum.

## References

- ANSI 2000 *American National Standard for the Safe Use of Lasers* ANSI Standard Z136.1
- Diebold G J, Sun T and Khan M I 1992 Photoacoustic waveforms generated by fluid bodies *Photoacoustic and Photothermal Phenomena III* ed D Bicanic (Berlin: Springer) pp 263–9
- Esenaliev R O, Tittel F K, Thomsen S L, Fornage B, Stelling C, Karabutov A A and Oraevsky A A 1997 Laser optoacoustic imaging for breast cancer diagnostics: limit of detection and comparison with X-ray and ultrasound imaging *Proc. SPIE* **2979** 71–82
- Esenaliev R O, Karabutov A A and Oraevsky A A 1999 Sensitivity of laser opto-acoustic imaging in detection of small deeply embedded tumors *IEEE J. Sel. Top. Quantum Electron.* **5** 981–8
- Gusev V E and Karabutov A A 1993 *Laser Optoacoustics* (New York: American Institute of Physics)
- Hoelen C G A and de Mul F F M 2000 Image reconstruction for photoacoustic scanning of tissue structures *Appl. Opt.* **39** 5872–83
- Hoelen C G A, de Mul F F M, Pongers R and Dekker A 1998 Three-dimensional photoacoustic imaging of blood vessels in tissue *Opt. Lett.* **23** 648–50
- Karabutov A A, Savateeva E V and Oraevsky A A 1999 Imaging of layered structures in biological tissues with opto-acoustic front surface transducer *Proc. SPIE* **3601** 284–95
- Karabutov A A, Savateeva E V, Podymova N B and Oraevsky A A 2000 Backward mode detection of laser-induced wide-band ultrasonic transients with optoacoustic transducer *J. Appl. Phys.* **87** 2003–14
- Kostli K P, Frenz M, Bebie H and Weber H P 2001 Temporal backward projection of optoacoustic pressure transients using Fourier transform methods *Phys. Med. Biol.* **46** 1863–72
- Kruger R A, Kiser W L, Miller K D, Reynolds H E, Reinecke D R, Kruger G A and Hofacker P J 2000 Thermoacoustic CT: imaging principles *Proc. SPIE* **3916** 150–9
- Kruger R A, Liu P, Fang Y R and Appledorn C R 1995 Photoacoustic ultrasound (PAUS)—Reconstruction tomography *Med. Phys.* **22** 1605–9
- Kruger R A, Reinecke D R and Kruger G A 1999 Thermoacoustic computed tomography—technical considerations *Med. Phys.* **26** 1832–7
- Ku G and Wang L-H 2000 Scanning thermoacoustic tomography in biological tissue *Med. Phys.* **27** 1195–202
- Ku G and Wang L-H 2001 Scanning microwave-induced thermoacoustic tomography: signal, resolution, and contrast *Med. Phys.* **28** 4–10
- Nelson S J and Soonmee Cha 2003 Imaging glioblastoma multiforme *J. Cancer* **9** 134–46
- Oraevsky A A, Andreev V A, Karabutov A A, Fleming D R, Gatalica Z, Singh H and Esenaliev R O 1999 Laser opto-acoustic imaging of the breast: detection of cancer angiogenesis *Proc. SPIE* **3597** 352–63
- Wang X, Pang Y, Ku G, Stoica G and Wang L-H 2003 Three-dimensional laser-induced photoacoustic tomography of the mouse brain with the skin and skull intact *Opt. Lett.* **28** 1739–41
- Xu Y, Feng D and Wang L-H 2002a Exact frequency-domain reconstruction for thermoacoustic tomography: I. Planar geometry *IEEE Trans. Med. Imaging* **21** 823–8
- Xu M and Wang L-H 2002 Time-domain reconstruction for thermoacoustic tomography in a spherical geometry *IEEE Trans. Med. Imaging* **21** 814–22
- Xu M and Wang L-H 2003 Analytic explanation of spatial resolution related to bandwidth and detector aperture size in thermoacoustic or photoacoustic reconstruction *Phys. Rev. E* **67** 056605
- Xu Y, Xu M and Wang L-H 2002b Exact frequency-domain reconstruction for thermoacoustic tomography: II. Cylindrical geometry *IEEE Trans. Med. Imaging* **21** 829–33
- Xu M H, Xu Yuan and Wang L-H V 2003 Time-domain reconstruction algorithms and numerical simulations for thermoacoustic tomography in various geometries *IEEE Trans. Biomed. Eng.* **50** 1086–99
- Zhulina Y V 2000 Optimal statistical approach to optoacoustic image reconstruction *Appl. Opt.* **39** 5971–7